Rock and Soil Mechanics

Volume 44 | Issue 2 Article 4

4-10-2023

Model test and finite beam element solution of cyclic lateral characteristics of piles in sloping ground

Wen-zhe PENG
College of Civil Engineering, Hunan University, Changsha, Hunan 410082, China Key Laboratory of Building Safety and Energy Efficiency of the Ministry of Education, Hunan University, Changsha, Hunan 410082, China

Ming-hua ZHAO
College of Civil Engineering, Hunan University, Changsha, Hunan 410082, China Key Laboratory of Building Safety and Energy Efficiency of the Ministry of Education, Hunan University, Changsha, Hunan 410082, China

Chao-wei YANG
College of Civil Engineering, Hunan University, Changsha, Hunan 410082, China Key Laboratory of Building Safety and Energy Efficiency of the Ministry of Education, Hunan University, Changsha, Hunan 410082, China

Heng ZHAO
College of Civil Engineering, Hunan University, Changsha, Hunan 410082, China Key Laboratory of Building Safety and Energy Efficiency of the Ministry of Education, Hunan University, Changsha, Hunan 410082, China

Rock and Soil Mechanics 2023 44(2): 381−391 ISSN 1000−7598
https: //doi.org/10.16285/j.rsm.2022.5186 http://rocksoilmech.researchcommons.org/journal

Model test and finite beam element solution of cyclic lateral characteristics of piles in sloping ground

PENG Wen-zhe[1, 2], ZHAO Ming-hua[1, 2], YANG Chao-wei[1, 2], ZHAO Heng[1, 2]

1. College of Civil Engineering, Hunan University, Changsha, Hunan 410082, China

2. Key Laboratory of Building Safety and Energy Efficiency of the Ministry of Education, Hunan University, Changsha, Hunan 410082, China

Abstract: To reveal the cyclic lateral characteristics of piles in sloping ground under the combined influence of slope effect and cyclic weakening effect, one-way cyclic lateral loading tests with different cycle numbers, load amplitudes and slope angles were carried out, and corresponding lateral static loading tests were conducted as a comparison. The variation trends of pile head deflection, bending moment and subgrade reaction were revealed. Then, the element stiffness matrix was improved by considering the second-order effect and pile-soil interaction to develop the finite beam element solution. Finally, the theoretical predicted curves were compared with measured curves and results calculated by the power series method to validate the finite beam element solution. The results show that the bending moments and pile deflections nonlinearly increase with cycle numbers, and the location of maximum bending moments gradually drops downwards from the non-dimensional depth z_α=1.25 to z_α=1.75. The relationship between the non-dimensional deflection $y_{0,\alpha}$ atop the pile and cycle number n satisfies the power function $y_{0,\alpha}=An^{0.11}$. When the load amplitude increases from 20 N to 40 N, the maximum non-dimensional bending moment increases from 0.010 to 0.029, but their locations remain near z_α=1.7. When the slope angle increases from 30° to 60°, the maximum non-dimensional bending moment increases from 0.011 (z_α=1) to 0.025 (z_α=2.5).

Keywords: bridge engineering; pile foundation; cyclic lateral characteristics; model test; slope effect; finite beam element method

1 Introduction

As the construction of China's transportation infrastructure continues to advance to the west, the number of highway/railway bridges crossing mountainous areas is increasing gradually. Meanwhile, pile foundations are widely used in highway/railway bridge projects in mountainous areas. They are often constructed in sloping ground (i.e., pile in sloping ground), and their force–deformation characteristics are affected by the slope effect[1–2]. During the service of highway/railway bridges, piles in sloping ground need to not only withstand the self-weight of the superstructure of the bridge, but also bear the cyclic lateral load caused by vehicle braking and strong winds. Therefore, the mechanical characteristics of piles in sloping ground are quite complex. The influence of slope effect and cyclic lateral load should be considered comprehensively in engineering design. It is not appropriate to copy the design calculation method of conventional bridge pile foundations.

At present, the force–deformation characteristics and the calculation methods for piles in sloping ground have gradually attracted the attention of engineering and academic fields. The key lies in revealing the influence of slope effect on the reduction of the subgrade reaction through field or model tests, and then developing a simplified analysis model of piles in sloping ground and the corresponding calculation method. In this regard, Zhao et al.[3] carried out a long-term research work. They established a simplified mechanical model of piles in sloping ground under inclined eccentric loads, and derived the finite difference solution of the internal force and deformation of piles in sloping ground by taking the load-bearing and anti-slip function of piles in sloping ground into account. Subsequently, according to the measured bending moments and deformations of the model tests, Liu et al.[4] revealed the evolution of subgrade reaction with pile top load. Zhao et al.[1] further deduced the finite beam element solution of pile responses in sloping ground. By improving the traditional strain wedge model, Peng et al.[5] developed a calculation method of subgrade reaction suitable for the engineering design of piles in sloping ground. In addition, based on model tests, Liu et al.[6] and Cheng et al.[7] proposed simplified design methods for the bearing capacity of laterally loaded piles in sloping ground, which comprehensively considered the influence of steep slope effect. Gao et al.[8] revised the shallow ultimate subgrade reaction, and derived the expression of the hyperbolic p–y curve under slope conditions according to the measured subgrade reaction–displacement (p–y) curve. Yu et al.[9] conducted model and revealed the nonlinear fitting relationship between the proportional coefficient m of the subgrade reaction coefficient of gravel soil and the slope grade. Yin et al.[10–11] revised the p–y curve for cohesive and sand slopes, and derived the finite difference solutions of the internal force and deformation of piles in sloping ground, and then, developed a simplified calculation method for the horizontal bearing capacity of piles in sloping ground at different slope grades based on the measured bending moments and deformations of the pile. Evidently, the above- mentioned research focuses on analyzing the influence of slope effect on the

Received: 18 February 2022 Accepted: 1 May 2022
This work was supported by the National Natural Science Foundation of China(52108317, 51908208).
First author: PENG Wen-zhe, male, born in 1993, PhD, research interests: pile foundation. E-mail: wzpeng@hnu.edu.cn
Corresponding author: YANG Chao-wei, male, born in 1988, PhD, Engineer, research interests: pile foundation. E-mail: cwyang@hnu.edu.cn

horizontal bearing capacity of piles or the subgrade reaction. However, the cyclic lateral characteristics of piles have not been involved.

As for the study of cyclic lateral characteristics, in general, the internal force–deformation evolution is revealed through model or field tests, and then a simplified calculation method of the foundation pile response is proposed considering the load characteristics, the number of cycles, and the load amplitude. The results of centrifugal model tests conducted in different types of soil indicate that the foundation pile deformation will show cumulative characteristics with the increase of the number of cycles[12], and the horizontal displacement and pile bending moment will increase[13]; the initial stiffness of the load–displacement curve and horizontal bearing capacity of the foundation pile increase with the increase of the relative pile–soil stiffness[14]. In addition, Chen et al.[15] introduced a cyclic effect coefficient to modify the *p–y* curve method based on cyclic lateral load tests of monopile in saturated silt to consider the effect of cyclic loading on the horizontal stiffness of the pile–soil system. Combining Poulos degradation model or backbone by API and Masing rules, Zhu et al.[16] and Yu et al.[17] constructed hyperbolic *p–y* curves under cyclic lateral loading based on field and model tests of cyclic lateral loading in soft clay, respectively. Based on the field tests, Wei et al.[18] proposed two power function relationships of proportional coefficient *m* of the subgrade reaction coefficient with the pile displacement at the ground surface and the number of cycles, respectively. Hu et al.[19] established a stiffness degradation model of the pile–soil system considering the cyclic weakening effect of sand. By introducing the concept of cyclic reaction ratio, they obtained the stiffness degradation factor of the pile–soil system, and then developed a modified *p-y* curve method which can consider the load characteristics, the number of cycles, and the cyclic weakening of sand stiffness. In summary, the research about cyclic lateral characteristics of pile are mostly focused on the flat ground, and the research results are difficult to guide the engineering design of piles in sloping ground under cyclic lateral loads.

Therefore, this paper intends to investigate the variation of the horizontal displacement, bending moment, and subgrade reaction of piles under different load characteristics, numbers of cycles, load amplitudes, and slope grades by model tests. Then, the cyclic lateral characteristics of piles in sloping ground are revealed under the joint influence of slope effect and cyclic weakening effect. Finally, based on the finite beam element method, considering the cyclic weakening effect of the proportional coefficient *m* of the subgrade reaction coefficient, a simplified calculation method for the internal force and deformation of piles in sloping ground under horizontal cyclic load is developed. The results are expected to provide a concise and effective analysis method for the preliminary design of pile foundations for bridge projects in mountainous areas.

2 Test scheme

To investigate the cyclic lateral characteristics of piles in sloping ground, a series of unidirectional cyclic lateral load model tests were conducted with different cycle numbers, load amplitudes and slope grade conditions. Meanwhile, horizontal static load tests under flat and slope conditions were carried out as a contrast, as shown in Table 1.

Table 1 Test program

Test type	No.	Loading mode	Amplitude /N	Slope grade /(°)
Horizontal static load test	S1	Slow-speed maintenance load	—	0
	S2		—	45
Unidirectional cyclic lateral load test	C1	Cyclic lateral load (n=2 500)	30	30
	C2		30	45
	C3		30	60
	C4		20	45
	C5		40	45

The above model tests were conducted in the geotechnical engineering laboratory of Hunan University using a pile foundation as prototype in sloping ground in Hunan Province as the prototype. The similarity criteria were derived by the equation analysis method as follows[4, 10–11]:

The fourth-order deflection differential equations for the prototype pile and the model pile under inclined load can be expressed respectively as:

$$E_{\mathrm{p}}I_{\mathrm{p}}\frac{\mathrm{d}^4y_{\mathrm{p}}}{\mathrm{d}z_{\mathrm{p}}^4}+N_{\mathrm{p}}\frac{\mathrm{d}^2y_{\mathrm{p}}}{\mathrm{d}z_{\mathrm{p}}^2}+b_{\mathrm{p}}m_{\mathrm{p}}z_{\mathrm{p}}y_{\mathrm{p}}=0 \tag{1}$$

$$E_{\mathrm{m}}I_{\mathrm{m}}\frac{\mathrm{d}^4y_{\mathrm{m}}}{\mathrm{d}z_{\mathrm{m}}^4}+N_{\mathrm{m}}\frac{\mathrm{d}^2y_{\mathrm{m}}}{\mathrm{d}z_{\mathrm{m}}^2}+b_{\mathrm{m}}m_{\mathrm{m}}z_{\mathrm{m}}y_{\mathrm{m}}=0 \tag{2}$$

where *EI* is the pile flexural stiffness; *y* is the pile deflection; *z* is the depth; *N* is the vertical load at the pile top; *b* is the calculation width of the pile; *m* is the proportional coefficient of the subgrade reaction coefficient; subscripts p and m represent the prototype and model, respectively.

The similar constants of these physical and mechanical parameters are $\lambda_b=b_{\mathrm{p}}/b_{\mathrm{m}}$, $\lambda_z=z_{\mathrm{p}}/z_{\mathrm{m}}$, $\lambda_{EI}=(E_{\mathrm{p}}I_{\mathrm{p}})/(E_{\mathrm{m}}I_{\mathrm{m}})$, $\lambda_m=m_{\mathrm{p}}/m_{\mathrm{m}}$ and $\lambda_N=N_{\mathrm{p}}/N_{\mathrm{m}}$. Substituting these similar constants to Eq. (1) yields

$$\frac{\lambda_{EI}\lambda_y}{\lambda_z^4}\cdot E_{\mathrm{m}}I_{\mathrm{m}}\frac{\mathrm{d}^4y_{\mathrm{m}}}{\mathrm{d}z_{\mathrm{m}}^4}+\frac{\lambda_N\lambda_y}{\lambda_z^2}\cdot\frac{\mathrm{d}^2y_{\mathrm{m}}}{\mathrm{d}z_{\mathrm{m}}^2}+\lambda_b\lambda_m\lambda_z\lambda_y bmzy=0 \tag{3}$$

Comparing Eq. (2) with Eq. (3), the following similarity criterion can be derived:

$$\frac{\lambda_{EI}\lambda_y}{\lambda_z^4}=\frac{\lambda_N\lambda_y}{\lambda_z^2}=\lambda_b\lambda_m\lambda_z\lambda_y \tag{4}$$

Based on the above similarity criterion and the similarity ratio in Table 2, a similarity index of 0.97 can be obtained (see Eq. (5)). It indicates that the model test results can provide a reference for the engineering prototype and can reveal to a certain extent the cyclic lateral characteristics of piles in

sloping ground under the joint influence of slope effect and cyclic weakening effect.

$$\kappa = \frac{\lambda_m \lambda_b \lambda_z^5}{\lambda_{EI}} = 0.97 \quad (5)$$

Table 2 Similarity ratios of physical and mechanical parameters

Type	Calculation width /m	Buried depth /m	Elastic modulus /GPa	Flexural stiffness /(kN • m^2)	Proportional coefficient of subgrade reaction coefficient /(MN • m^{-3})
Prototype	2.700 0	25.00	29.60	2.43×10^7	35.42
Model test	0.065 7	1.00	1.16	4.31×10^{-2}	26.24
Similarity ratio	41.10	25.00	25.52	5.56×10^8	1.35

The dimension of the test box is 1.6 m×1 m×1.2 m, and its front and back are composed of transparent glass. The maximum horizontal distance between the model pile and the test box wall is about 35 times the pile diameter, its direction is parallel to the loading direction, and the distances in the other three directions are about 15 times the pile diameter, which can better avoid boundary effects[8, 20] (see Fig. 1). The modified Polypropylene random copolymer pipe (PPR pipe) with an outer diameter of 32 mm and a wall thickness of 4.4 mm was used for the model pile, and it was set into a sleeve welded to the bottom plate of the test box to fix the pile (buried at a depth of 1 m). To obtain accurate response of the foundation pile, multiple sets of strain gauges (BFH120-5AA-D150) and earth pressure cells (DMTY type) were installed symmetrically along the length of the model pile, and a displacement meter (DMWY-100) was installed at the top of the pile, as shown in Figs. 1 and 2. The model slope is a sandy (river sand) slope with a unit weight γ of 18.83 kN/m^3, a specific gravity G_s of 2.62, an internal friction angle φ of 13.26°, an apparent cohesion c of 10.66 kPa, a water content ω of 3.84%, a void ratio e of 0.42, a compression modulus $E_{s,1-2}$ of 4.43 MPa, an uniformity coefficient C_u of 5.74 and a coefficient of curvature C_c of 0.94. The ratio of the pile diameter and the particle diameter d_{50} (the diameter through which 50% of the total soil mass is passing) is about 50, greater than the minimum requirement of 40[8]. Therefore, the influence of size effect can be neglected.

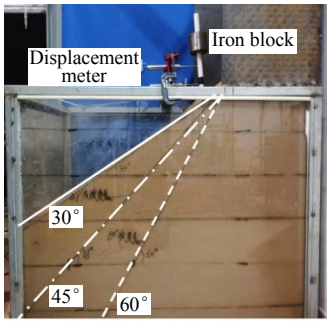

Fig. 1 Model pile and slope

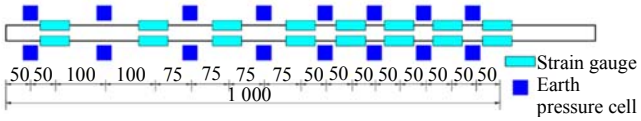

Fig. 2 Strain gauges and earth pressure cells (unit: mm)

In the model tests, the vertical load was provided by an iron block at the top of the pile and maintained at a constant of 80 N. The horizontal static load tests adopted the slow-speed maintenance load method for loading in increment with an increment of 10 N. The unidirectional cyclic lateral load tests adopted the T-wave loading path for cyclic loading (with a period of 30 s). During the tests, the horizontal displacement y_0 at the top of the pile and the subgrade reaction p can be measured directly by the displacement meter and earth pressure cells, respectively. The pile bending moment M can be deduced from the measured strain of each group of strain gauges.

In addition, to make the experimental and theoretical results of this study more general, four dimensionless parameters were introduced for analysis, i.e., dimensionless displacement y_α, dimensionless bending moment M_α, dimensionless subgrade reaction p_α and dimensionless depth z_α.

$$y_\alpha = y/b \quad (6)$$

$$M_\alpha = M/\alpha EI \quad (7)$$

$$p_\alpha = p/\alpha^3 EI \quad (8)$$

$$z_\alpha = \alpha z \quad (9)$$

where α is the deformation coefficient of the pile[21], $\alpha = (mb/EI)^{1/5}$.

3 Analysis of model test results

3.1 Horizontal static load test

The relationships between the horizontal static load and lateral displacement atop the pile for the horizontal static load tests S1 (flat ground) and S2 ($\theta = 45°$) are shown in Fig.3. It shows that the $P_0 - y_0$ curves can be fitted by power functions for both flat ground and slope conditions, $P_0 = 19.45\, y_0^{0.63}$ ($y_0 = 0.01\, P_0^{1.54}$) for flat ground and $P_0 = 14.82\, y_0^{0.59}$ ($y_0 = 0.008\, P_0^{1.76}$) for sloping ground. We take the critical lateral displacement of pile top as 5.89 mm (about 0.2 times the pile diameter), the horizontal bearing capacities P_{cr} of the model piles of tests S1 and S2 are 60 N and 40 N, respectively. The relationships between the bending moment at the ground surface and lateral load atop the pile for the horizontal static load tests S1 and S2 are presented in Fig. 4. One can see that the $M_0 - P_0$ curves can be fitted by the elementary functions, $M_0 = 0.01\, P_0 + 0.004\,4\, P_0^{1.54}$ for the flat ground and $M_0 = 0.01\, P_0 + 0.002\,9\, P_0^{1.76}$ for the slope condition. Evidently, the pile bending moment at the ground surface consists of two parts. The former $0.01P_0$ is caused by the lateral load eccentricity (with an eccentric distance of 0.01 m) and the latter $0.004\,4\, P_0^{1.54}$ or $0.002\,9\, P_0^{1.76}$ is caused by the

second order effect. In addition, under the same horizontal static load condition, both the lateral displacement atop the pile and the pile bending moment at the ground surface under the slope condition are significantly larger than those under the flat ground condition. It indicates that the slope effect will significantly affect the pile response and reduce the horizontal bearing capacity of the pile, which should be given full attention in the design of mountainous highway/railway bridge projects.

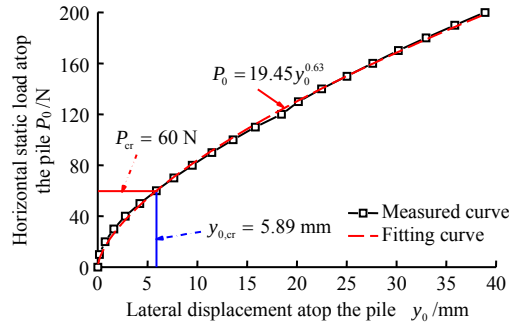

(a) Flat ground (S1)

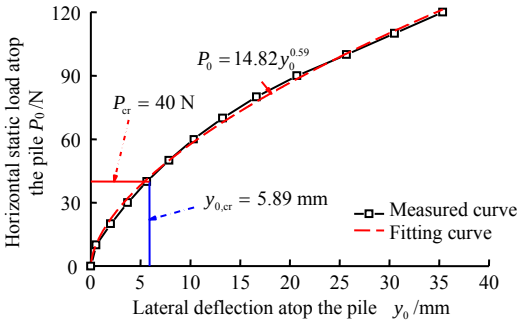

(b) Sloping ground (S2)

Fig. 3 Lateral load versus deflection atop the pile

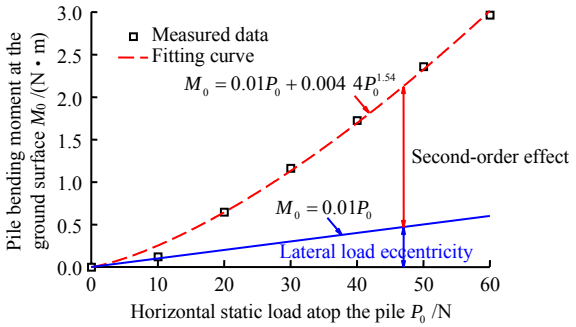

(a) Flat ground (S1)

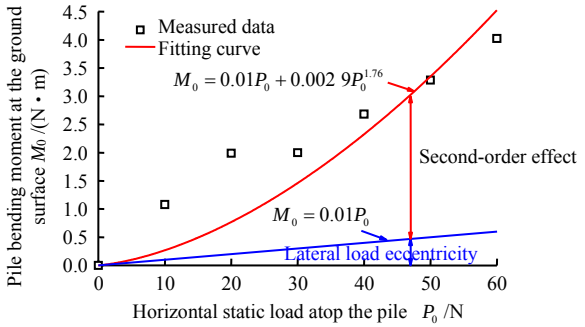

(b) Sloping ground (S2)

Fig. 4 Bending moment at the ground surface versus lateral load atop the pile

3.2 Cyclic lateral load test

As shown in Fig. 5, as the cycle number n increases, the dimensionless displacement $y_{0,\alpha}$ atop the pile in the cyclic lateral load test increases nonlinearly, and the rate of increase decreases gradually. After the first 100 cycles of loading, the dimensionless displacement atop the pile can reach 60% of that at the last cycle of loading ($n = 2\ 500$). That is to say, the response of piles in sloping ground under cyclic lateral loading is controlled by the first 100 cycles of loading. In addition, the pile head dimensionless displacement–cycle number curve can also be fitted by a power function $y_{0,\alpha} = An^{0.11}$ [22], where A is a fitting coefficient, depending on the pile head dimensionless displacement $y_{0,s}/b$, slope grade θ and load amplitude P_0 in the corresponding horizontal static load test. Obviously, the fitting effect of such power functions is better, and the exponents of cycle number are all 0.11. It can provide some reference for the prediction of lateral displacement atop the pile under cyclic lateral loading conditions.

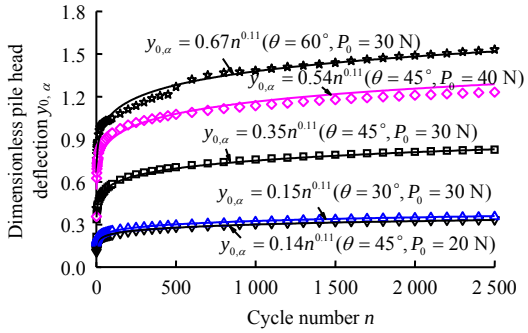

Fig. 5 Dimensionless pile head deflection versus cycle number

To investigate the variation of pile bending moment M with the cycle number n, the variation curves of dimensionless bending moment with the cycle number at different depths are compared, as shown in Fig. 6. It can be seen that when $z_\alpha < 4.58$, the dimensionless bending moment increases nonlinearly with the cycle number, and the increase rate decreases significantly when the cycle number n exceeds 100; as a contrast, when $z_\alpha > 4.58$, the dimensionless bending moment remains almost constant and is not affected by the cycle number. It indicates that the subgrade reaction above depth $z_\alpha = 4.58$ can resist the cyclic lateral load.

In addition to the cycle number, the response of piles in sloping ground is also closely related to the load amplitude and slope grade. For example, the dimensionless displacement of the pile top in Fig. 5 is positively related to the load amplitude and slope grade. To further explore the effects of load amplitude and slope grade on the response of piles in sloping ground under cyclic lateral loading conditions, the cycle number n is taken to be constant at 100, the dimensionless bending moment and subgrade reaction distribution under different load amplitudes and slope grades are compared in Fig. 7.

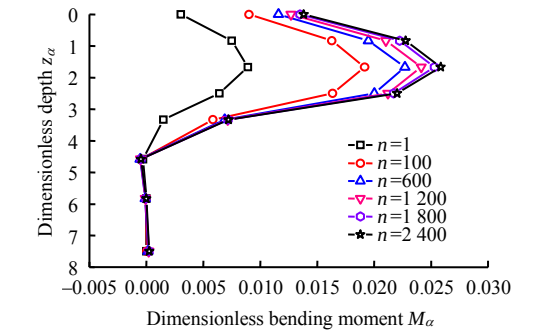

(a) Dimensionless depth–dimensionless bending moment

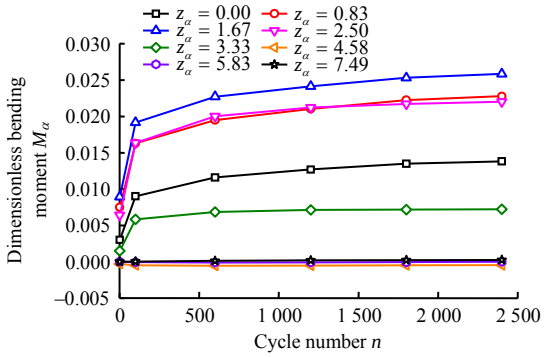

(b) Dimensionless bending moment–cycle number

Fig. 6 Variation of dimensionless bending moments under different cycle numbers

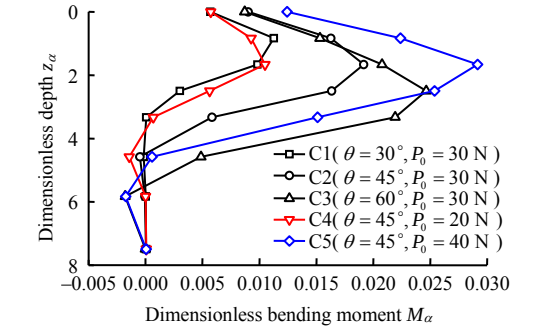

(a) Dimensionless depth–dimensionless bending moment

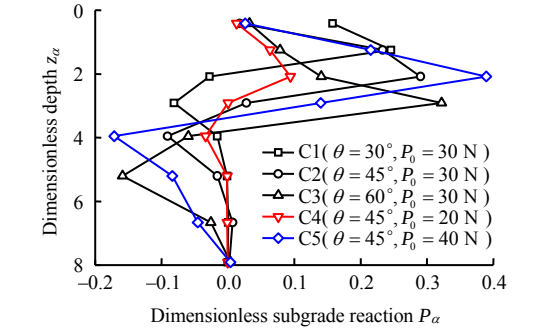

(b) Dimensionless depth–dimensionless subgrade reaction

Fig. 7 Dimensionless bending moment and subgrade reaction profiles under different load amplitudes and slope angles (n=100)

When the load amplitude increases from 20 N to 30 N and 40 N, the maximum dimensionless bending moment increases from 0.010 to 0.019 and 0.029, and its position remains unchanged, located near $z_\alpha = 1.7$. At the same time, the maximum dimensionless subgrade reaction increases from 0.094 to 0.290 and 0.441, and its position also remains the same, located near $z_\alpha = 2$. In addition, when the slope grade increases from $\theta = 30°$ to $\theta = 45°$ and $\theta = 60°$, the maximum dimensionless bending moment increases from 0.011 to 0.019 and 0.025, which appears near $z_\alpha = 1.0$, 1.7 and 2.5, respectively. At the same time, the maximum dimensionless subgrade reaction increases from 0.246 to 0.290 and 0.322, which appears near $z_\alpha = 1.25$, 2.00 and 2.91, respectively. Evidently, both the maximum bending moment and subgrade reaction increase with the increase of the load amplitude and slope grade. That is to say, the pile displacement increases with the increase of load amplitude and slope grade, and the maximum subgrade reaction increases accordingly. The inflection point ($M = 0$) and displacement-zero point ($y = 0$) both shift downward with the increase of the slope grade. It is because when the slope grade is larger, deeper subgrade reaction needs to be mobilized to resist the cyclic lateral load in order to maintain the pile equilibrium.

It is not difficult to find that the depth–displacement curve is usually more difficult to be measured directly than lateral displacement atop the pile, pile bending moment and subgrade reaction distribution due to the limitation of test conditions and instruments. Therefore, some researchers try to use the elementary function to fit the measured bending moment and then carry out the second-order integration (Eq. (10)) to derive the pile lateral displacement, such as the local fifth spline function[23], the cubic function[24] (Eq. (11)) and the elementary function[25] (Eq. (12)).

$$y(z)=\frac{1}{EI}\left\{\iint\left[M(z)\mathrm{d}z\right]\mathrm{d}z\right\} \tag{10}$$

$$M(z)=A_M z^3+B_M z^2+C_M z+D_M \tag{11}$$

$$M(z)=-\frac{\mathrm{e}^{-\beta z}P_0}{\beta}\left[\sin\beta z+e\beta\left(\cos\beta z+\sin\beta z\right)\right] \tag{12}$$

However, the pile response derived based on the above bending moment fitting function may not be consistent with reality. For example, the subgrade reaction distribution obtained by second-order differentiation based on the third-order function is a linear function[24], which does not conform to the actual subgrade reaction distribution variation. For this reason, it is necessary to propose a concise and effective theoretical calculation method to analyze the response of piles in sloping ground under cyclic lateral loading conditions.

4 Finite beam element method and verification

4.1 Basic principle

The finite beam element method (FBEM) is widely used in the force and deformation analysis of piles, columns and other rod structures and their combinations[1, 5]. Its basic principles are described as follows. (i) The research object is discretized into several beam elements

according to the design accuracy requirements. (ii) The load and displacement column vectors and element stiffness matrices in local coordinates are established. (iii) The element stiffness matrix is integrated into the overall stiffness matrix, and then the internal force and deformation of the beam element are solved. As shown in Fig. 8, the end points i and j of the beam element are subjected to vertical loads $\overline{F}_{Ni}$ and $\overline{F}_{Nj}$, horizontal loads $\overline{F}_{Qi}$ and $\overline{F}_{Qj}$, and bending moments $\overline{M}_i$ and $\overline{M}_j$, respectively. The corresponding deformations of the end points of the beam element are vertical displacements $\overline{u}_i$ and $\overline{u}_j$, horizontal displacements $\overline{v}_i$ and $\overline{v}_j$, and angles of rotation $\overline{\varphi}_i$ and $\overline{\varphi}_j$.

Based on the matrix displacement method, the column vector $\overline{\boldsymbol{F}}^{\mathrm{e}}$ of endpoint forces and the column vector of endpoint displacements $\overline{\boldsymbol{\delta}}^{\mathrm{e}}$ of the beam element can be expressed as

$$\overline{\boldsymbol{F}}^{\mathrm{e}}=\left[\overline{F}_{Ni}\quad \overline{F}_{Qi}\quad \overline{F}_{Mi}\quad \overline{F}_{Nj}\quad \overline{F}_{Qj}\quad \overline{F}_{Mj}\right]^{\mathrm{T}} \tag{13}$$

$$\overline{\boldsymbol{\delta}}^{\mathrm{e}}=\left[\overline{u}_i\quad \overline{v}_i\quad \overline{\varphi}_i\quad \overline{u}_j\quad \overline{v}_j\quad \overline{\varphi}_j\right]^{\mathrm{T}} \tag{14}$$

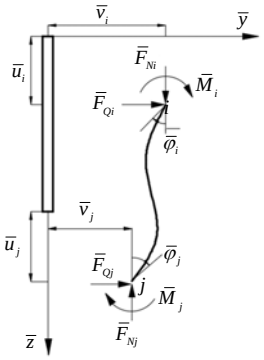

Fig. 8 Force and deformation analysis of beam elements

The shape functions of vertical displacement $u(\overline{z})$, horizontal displacement $v(\overline{z})$ and rotation angle $\varphi(\overline{z})$ of the beam element at depth $\overline{z}$ in local coordinates can be derived from the displacement boundary conditions, and their matrix forms are

$$u(\overline{z})=\left[1-\frac{\overline{z}}{l_i}\quad \frac{\overline{z}}{l_i}\right]\left[\overline{u}_i\quad \overline{u}_j\right]^{\mathrm{T}}=\boldsymbol{N}_u\cdot\overline{\boldsymbol{\delta}}^{\mathrm{e}} \tag{15}$$

$$v(\overline{z})=\left[1-\frac{3\overline{z}^2}{l_i^2}+\frac{2\overline{z}^3}{l_i^3}\quad x-\frac{2\overline{z}^2}{l_i}+\frac{\overline{z}^3}{l_i^2}\quad \frac{3\overline{z}^2}{l_i^2}-\frac{2\overline{z}^3}{l_i^3}\quad -\frac{\overline{z}^2}{l_i}+\frac{\overline{z}^3}{l_i^2}\right]\left[\overline{v}_i\ \ \overline{\varphi}_i\ \ \overline{v}_j\ \ \overline{\varphi}_j\right]^{\mathrm{T}}=\boldsymbol{N}_v\cdot\overline{\boldsymbol{\delta}}^{\mathrm{e}} \tag{16}$$

$$\varphi(\overline{z})=\left[-\frac{6\overline{z}}{l_i^2}+\frac{6\overline{z}^2}{l_i^3}\quad 1-\frac{4\overline{z}}{l_i}+\frac{3\overline{z}^2}{l_i^2}\quad \frac{6\overline{z}}{l_i^2}-\frac{6\overline{z}^2}{l_i^3}\quad -\frac{2\overline{z}}{l_i}+\frac{3\overline{z}^2}{l_i^2}\right]\left[\overline{v}_i\ \ \overline{\varphi}_i\ \ \overline{v}_j\ \ \overline{\varphi}_j\right]^{\mathrm{T}}=\boldsymbol{N}_\varphi\cdot\overline{\boldsymbol{\delta}}^{\mathrm{e}} \tag{17}$$

where $\boldsymbol{N}_u$, $\boldsymbol{N}_v$ and $\boldsymbol{N}_\varphi$ are the shape function matrices of the vertical displacement, horizontal displacement and rotation angle of the beam element, respectively; and l_i is the length of the beam element.

Due to the limitation of space, the derivation of the improved element stiffness matrix are not described in detail in this study, which can be found in reference [1]. In addition, the requirements of highway and railway industry specifications for the design of foundation piles are quite demanding and the m method is recommended by the specifications. Therefore, when taking into account the influence of the pile side soil in the finite beam element method, the m method is also used to consider the subgrade reaction around the pile, and subgrade reaction is converted to the beam element stiffness. Then, considering the second-order effect and the pile–soil interaction effect, the element stiffness matrix $\boldsymbol{k}$ can be expressed in the form of a symmetric matrix:

$$\boldsymbol{k}=\begin{bmatrix}
\frac{EA}{l_i} & 0 & 0 & -\frac{EA}{l_i} & 0 & 0\\
0 & \frac{12EI}{l_i^3}+\frac{p_{ij}}{l_i}+mb\left(h_i+\frac{l_i}{2}\right)\frac{13}{35}l_i & \frac{6EI}{l_i^2}+mb\left(h_i+\frac{l_i}{2}\right)\frac{11}{210}l_i & 0 & -\frac{12EI}{l_i^3}-\frac{p_{ij}}{l_i}+mb\left(h_i+\frac{l_i}{2}\right)\frac{9}{70}l_i & \frac{6EI}{l_i^2}-mb\left(h_i+\frac{l_i}{2}\right)\frac{13}{420}l_i^2\\
0 & \frac{6EI}{l_i^2}+mb\left(h_i+\frac{l_i}{2}\right)\frac{11}{210}l_i & \frac{4EI}{l_i}+mb\left(h_i+\frac{l_i}{2}\right)\frac{1}{105}l_i^3 & 0 & -\frac{6EI}{l_i^2}-mb\left(h_i+\frac{l_i}{2}\right)\frac{19}{140}l_i^2 & \frac{2EI}{l_i}-mb\left(h_i+\frac{l_i}{2}\right)\frac{1}{140}l_i^3\\
-\frac{EA}{l_i} & 0 & 0 & \frac{EA}{l_i} & 0 & 0\\
0 & -\frac{12EI}{l_i^3}-\frac{p_{ij}}{l_i}+mb\left(h_i+\frac{l_i}{2}\right)\frac{9}{70}l_i & -\frac{6EI}{l_i^2}-mb\left(h_i+\frac{l_i}{2}\right)\frac{19}{140}l_i^2 & 0 & \frac{12EI}{l_i^3}+\frac{p_{ij}}{l_i}+mb\left(h_i+\frac{l_i}{2}\right)\frac{13}{35}l_i & -\frac{6EI}{l_i^2}-mb\left(h_i+\frac{l_i}{2}\right)\frac{11}{210}l_i^2\\
0 & \frac{6EI}{l_i^2}-mb\left(h_i+\frac{l_i}{2}\right)\frac{13}{420}l_i^2 & \frac{2EI}{l_i}-mb\left(h_i+\frac{l_i}{2}\right)\frac{1}{140}l_i^3 & 0 & -\frac{6EI}{l_i^2}-mb\left(h_i+\frac{l_i}{2}\right)\frac{11}{210}l_i^2 & \frac{4EI}{l_i}+mb\left(h_i+\frac{l_i}{2}\right)\frac{1}{105}l_i^3
\end{bmatrix} \tag{18}$$

where EA is the tensile (compressive) stiffness; p_{ij} is the average force of the upper and lower end nodes of the beam element.

Based on the principle of virtual work, the relationship between the endpoint force column vector and the endpoint displacement column vector of the beam element can be deduced as

$$\overline{\boldsymbol{F}}^{\mathrm{e}}=\boldsymbol{k}\overline{\boldsymbol{\delta}}^{\mathrm{e}} \tag{19}$$

The element stiffness matrix of each beam element is superimposed into the overall stiffness matrix $\boldsymbol{K}$ according to the "end-to-end connection" principle, as

shown in Fig. 9. Since the element stiffness matrix is a 6×6 matrix, the pile is divided into N beam elements, and the global stiffness matrix has a total of order $(3N+3)\times(3N+3)$. Then, the matrix equation $\boldsymbol{\Delta}=\boldsymbol{K}^{-1}\cdot\boldsymbol{F}$ (Δ and $\boldsymbol{F}$ are the global displacement and load column vectors, respectively) can be used to solve the internal force and deformation of the foundation pile.

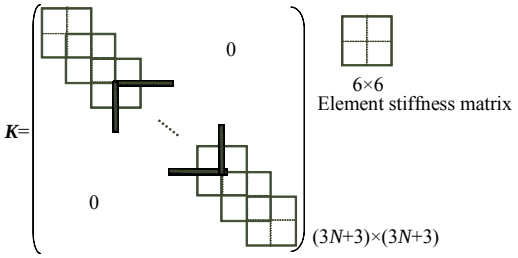

Fig. 9 Global stiffness matrix

4.2 Horizontal static load test

To verify the reasonableness of FBEM in the response analysis of foundation piles, the horizontal static load tests S1 (flat ground) and S2 (sloping ground) were taken as examples. The P_0-y_0 curves and dimensionless bending moment curves of piles predicted by FBEM were compared with the measured curves and calculation results by the power series method (PSM)[21], as shown in Figs. 10 and 11. The horizontal displacement and bending moment of the pile below dimensionless depth $z_\alpha=4$ are almost 0, which can be neglected[21]. As can be seen from Fig. 10,

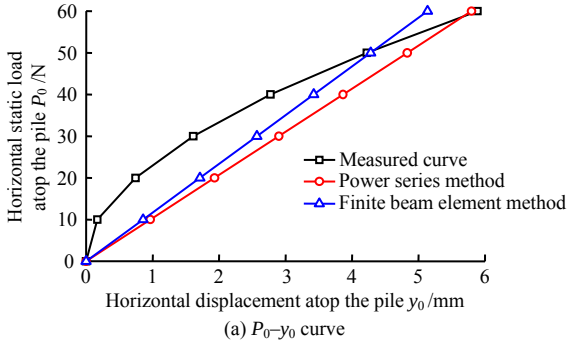

(a) P_0–y_0 curve

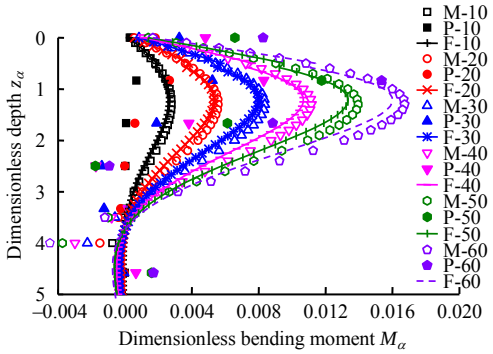

Notes: M represents the measured curve; P represents the power series method; F represents the finite beam element method; 10–60 represents the horizontal load 10–60 N.

(b) Dimensionless depth–dimensionless bending moment

Fig. 10 Comparisons of measured P_0–y_0 curves and Dimensional bending moment curves with those predicted by theoretical methods in test S1

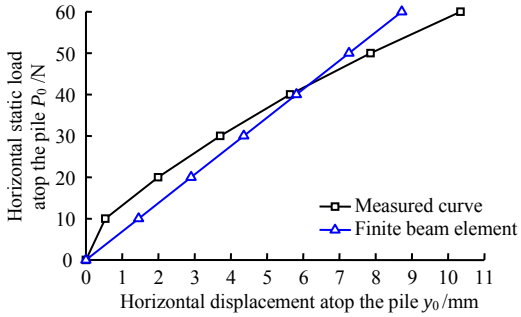

(a) P_0–y_0 curve

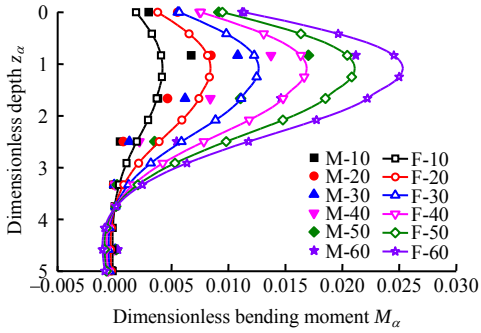

(b) Dimensionless bending moment curve

Fig. 11 Comparisons of measured P_0–y_0 curves and Dimensional bending moment curves with those predicted by theoretical methods in test S2

the predicted P_0-y_0 curve of FBEM matches well with the measured curve and the calculated P_0-y_0 curve of PSM. In addition, the variation trend of the dimensionless bending moment curves predicted by FBEM and PSM are consistent, and the maximum dimensionless bending moment and its location also match well. However, there is a certain error between the two and the measured curve. In addition to the measurement error, the error is due to the difference between the pile bending moment at the ground surface ($0.01\,P_0$) used in FBEM and PSM and the actual bending moment ($0.01\,P_0+0.004\,4\,P_0^{1.54}$). It also indicates that the second-order effect is not negligible in the pile response analysis and should be fully considered in the subsequent analysis (horizontal static load test S2 and cyclic lateral load tests C1 to C5).

Then, to account for the slope effect, the proportional coefficient m of the shallow subgrade reaction coefficient was revised to $m'=0.5m$ [2, 5, 21], and the FBEM-predicted foundation pile response was compared with the measured results, as shown in Fig. 11. Evidently, the FBEM predicted P_0-y_0 curve and dimensionless bending moment curve are consistent with the measured curves in terms of both values and variation trends. In summary, it is feasible to use FBEM to analyze the foundation pile response of horizontal static load tests under flat and slope conditions.

In addition, the FBEM-predicted horizontal displacements of the foundation piles for horizontal static load tests under flat and slope conditions are shown in Fig.12, and the corresponding measured dimensionless subgrade reaction distribution is shown in Fig.13.

Thus, the subgrade reaction–horizontal displacement curves (p–y curves) at different depths can be obtained as shown in Fig. 14. The slope of the curves in the figure can be regarded as the measured subgrade reaction modulus. It can be seen that the subgrade reaction modulus increases significantly with depth;

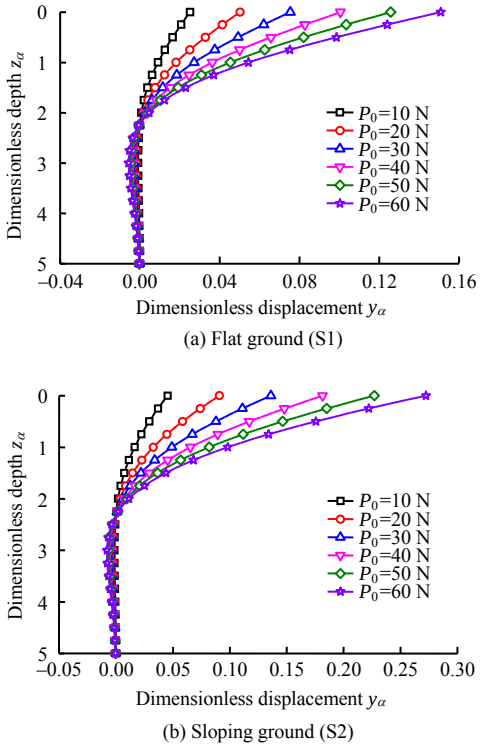

Fig. 12 Predicted dimensionless deflections in tests S1 and S2

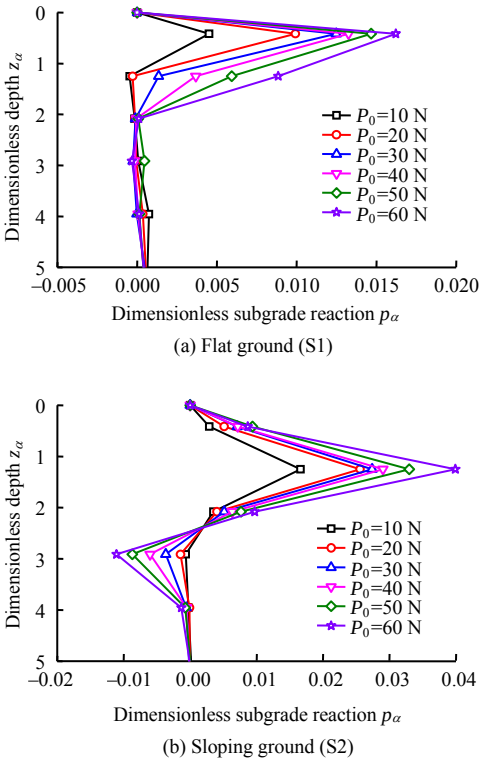

Fig. 13 Measured dimensionless subgrade reaction profiles in tests S1 and S2

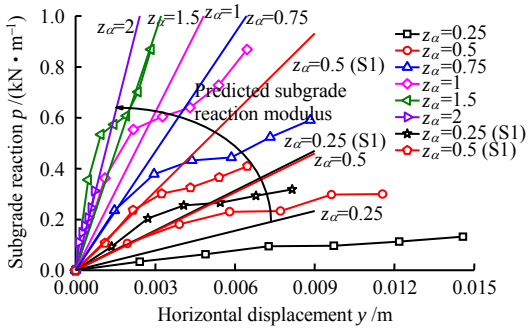

Fig. 14 Comparisons of measured subgrade reaction modulus and those employed in FBEM

when the depth is the same, the subgrade reaction modulus under the slope condition is smaller than that under the flat ground condition (such as $z_\alpha = 0.25$ and $z_\alpha = 0.5$). It indicates that the slope effect will lead to the decrease of the subgrade reaction modulus. In addition, the above p–y curves are close to the trend of the existing experimental results[23, 24, 26], and they are in good agreement with the adopted subgrade reaction modulus of FBEM (dashed and dotted lines in Fig. 14) within a certain range. It also proves the feasibility of FBEM to predict the horizontal static response of foundation piles in flat and slope conditions.

4.3 Cyclic lateral loading test

When using FBEM to analyze the response of piles in sloping ground under cyclic lateral loading conditions, the cyclic weakening effect of the subgrade reaction[12, 16] should be considered, similar to the slope effect[9, 26]. This can be achieved by appropriately discounting the proportional coefficient m of the subgrade reaction coefficient. Subsequently, by discounting m to different degrees for test C2, the response of piles in sloping ground is calculated by FBEM with different number of cycles, including dimensionless displacement curve (see Fig. 15(a)) and dimensionless bending moment curve (see Fig. 15(b)). Then, the dimensionless displacement–cycle number curves (see Fig. 16(a)) and dimensionless bending moment distribution curves (see Fig. 16(b)) atop the pile are compared with the measured data. Obviously, the theoretically predicted curves and the measured data are in good agreement. It indicates that, (i) it is feasible to consider the influence of cyclic weakening effect and slope effect by discounting m, and the reduction of m[9, 11, 18] satisfies the logarithmic attenuation relationship $m/m_0 = 1.34 - 0.16\ln(n + 7.13)$ (see Fig. 17), where m_0 is the value of m under the horizontal static load; (ii) FBEM can better predict the horizontal displacement of pile in sloping ground under cyclic lateral loading conditions. In addition, as the number of cycles n increases, the dimensionless bending moment gradually increases, and the position of the maximum dimensionless bending moment shifts down from $z_\alpha = 1.25$ to $z_\alpha = 1.75$. It indicates that the cumulative plastic strain increases with the number of cycles, and the strength of the soil around the pile gradually decreases. The horizontal load is transmitted to deeper positions along the pile. That is to say, the cyclic

lateral loading will lead to weakening of the shallow subgrade reaction modulus, prompting the mobilization of deeper subgrade reaction to maintain the pile equilibrium. Meanwhile, the inflection point ($M = 0$) will be shifted downward.

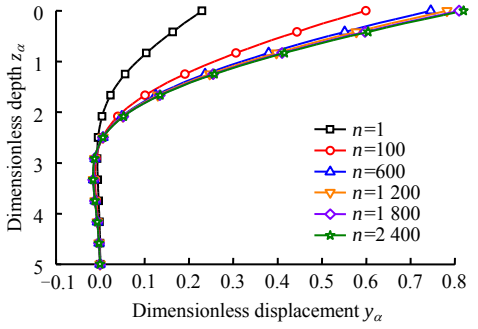

(a) Dimensionless displacement curve

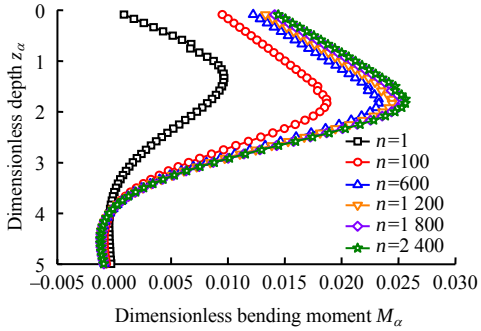

(b) Dimensionless bending moment curve

Fig. 15 Dimensionless pile deflections and dimensionless bending moments under different cycle numbers predicted by FBEM

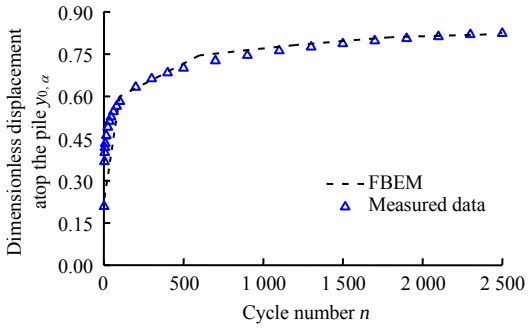

(a) Dimensionless displacement–cycle number atop the pile

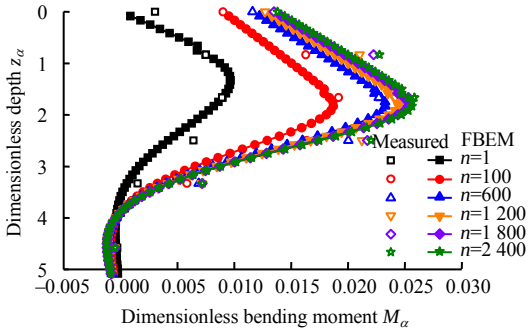

(b) Dimensionless bending moment curve

Fig. 16 Comparisons of dimensionless pile head deflection–cycle number curves, dimensionless bending moment curves predicted by FBEM with those measured in test C2

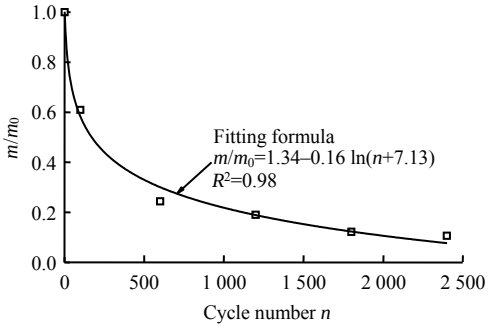

Fig. 17 Reductions of proportional coefficients under different cycle numbers

5 Conclusions

(1) The dimensionless displacement atop the pile increases nonlinearly with the number of cycles, and the increment ratio decreases gradually. The curve can be fitted by the power function $y_{0,\alpha} = An^{0.11}$. The response of piles in sloping ground under cyclic lateral loading condition is mainly controlled by the first 100 loading cycles.

(2) The variation curves of dimensionless displacement atop the pile and dimensionless bending moment predicted by the finite beam element method are in good agreement with the measured results. It indicates that the finite beam element method can better predict the horizontal displacement of piles in sloping ground under cyclic lateral loading conditions when adopting a suitable proportional coefficient of subgrade reaction coefficient.

(3) When the load amplitude increases from $P_0 =$ 20 N to $P_0 = 30$ N and $P_0 = 40$ N, the maximum dimensionless bending moment increases from 0.010 to 0.019 and 0.029, but its position remains unchanged near $z_\alpha = 1.7$. The maximum dimensionless subgrade reaction will increase from 0.094 to 0.290 and 0.441, and its position also remains unchanged near $z_\alpha = 2$. Both the maximum pile bending moment and subgrade reaction increase with the increase of load amplitude, that is, the pile displacement increases with the increase of load amplitude, resulting in an overall increase of subgrade reaction.

(4) When the slope grade increases from 30° to 45° and 60°, the maximum dimensionless bending moment increases from 0.011 to 0.019 and 0.025, located near $z_\alpha = 1.0$, 1.7 and 2.5, respectively; the maximum dimensionless subgrade reaction increases from 0.246 to 0.290 and 0.322, located near $z_\alpha = 1.25$, 2.00 and 2.91, respectively. Evidently, both the maximum pile bending moment and subgrade reaction increase with the increase of slope grade, that is to say, the pile displacement increases with the increase of grade, which leads to an overall increase of subgrade reaction. In addition, the inflection point ($M = 0$) and displacement-zero point both move down with the increase of grade.

References

[1] ZHAO Ming-hua, YANG Chao-wei, YANG Ming-hui, et al. Mechanical analysis of bridge pile foundation in high and steep slopes based on finite bar element method[J]. China Journal of Highway and Transport, 2014, 27(6): 51–58, 108.

[2] ZHAO Ming-hua, PENG Wen-zhe, YANG Chao-wei, et al. Finite difference solution of bridge double-pile structure on a steep transverse slope[J]. China Journal of Highway and Transport, 2019, 32(2): 87–96.

[3] ZHAO Ming-hua, LIU Jian-hua, YANG Ming-hui. Inner-force calculation of bridge pile foundation in high-steep rock slope under inclined loads[J]. Chinese Journal of Rock Mechanics and Engineering, 2006, 25(11): 2352–2357.

[4] LIU Jian-hua, ZHAO Ming-hua, YANG Ming-hui. Model tests on bridge pile foundation in high and steep rock slopes[J]. Chinese Journal of Geotechnical Engineering, 2009, 31(3): 372–377.

[5] PENG W Z, ZHAO M H, XIAO Y, et al. Analysis of laterally loaded piles in sloping ground using a modified strain wedge model[J]. Computers and Geotechnics, 2019, 107(3): 163–175.

[6] LIU Zi-sheng, ZHUO Yang, SHI Bei-ling, et al. Horizontal bearing capacity of pile foundation in high-piled wharf with inclined ground surface[J]. Chinese Journal of Geotechnical Engineering, 2010, 32(12): 1861–1867.

[7] CHENG Liu-yong, XU Xi-chang, CHEN Shan-xiong, et al. Model test and numerical simulation of horizontal bearing capacity and impact factors for foundation piles in slope[J]. Rock and Soil Mechanics, 2014, 35(9): 2685–2691.

[8] GAO Bo-lei, ZHANG Chen-rong, ZHANG Zhao-xu. Model tests on effect of slopes on lateral resistance of near single piles in sand[J]. Rock and Soil Mechanics, 2014, 35(11): 3191–3198.

[9] YU Hao-jun, PENG She-qin, ZHAO Qi-hua, et al. Study on coefficient of horizontal resistance for gravel soil foundation on slope[J]. Rock and Soil Mechanics, 2017, 38(6): 1682–1687, 1704.

[10] YIN Ping-bao, NIE Dao-liu, YANG Zhao-hui, et al. The *p-y* curve and computation method of the horizontal bearing capacity of piles in sloping ground[J]. Chinese Journal of Rock Mechanics and Engineering, 2018, 37(4): 996–1003.

[11] YIN Ping-bao, HE Wei, ZHANG Jian-ren, et al. Study on spatial effect of slope and horizontal bearing behavior of piles in sloping ground[J]. China Civil Engineering Journal, 2018, 51(4): 94–101.

[12] WANG Fu-qiang, RONG Bing, ZHANG Ga, et al. Centrifugal model test of pile foundation for wind power unit under cyclic lateral loading[J]. Rock and Soil Mechanics, 2011, 32(7): 1926–1930.

[13] DING Chu, YU Wen-rui, SHI Jiang-wei, et al. Centrifuge studies of pile deformation mechanisms due to lateral cyclic loading[J]. Rock and Soil Mechanics, 2020, 41(8): 2659-2664, 2711.

[14] LI Sen, YU Jian, HUANG Mao-song. Centrifuge test on single pile with different rigidities in saturated clay under cyclic lateral loading[J]. Chinese Journal of Geotechnical Engineering, 2021, 43(5): 948–954.

[15] CHEN Ren-peng, GU Ming, KONG Ling-gang, et al. Large-scale model tests on high-rise platform pile groups under cyclic lateral loads[J]. Chinese Journal of Geotechnical Engineering, 2012, 34(11): 1990–1996.

[16] ZHU Bin, YANG Yong-yao, YU Zhen-gang, et al. Field tests on lateral monotonic and cyclic loading of offshore elevated piles[J]. Chinese Journal of Geotechnical Engineering, 2012, 34(6): 1028–1037.

[17] YU Jian, HUANG Mao-song, ZHANG Chen-rong. Model tests and analysis of single piles with two different diameters subjected to cyclic lateral loading in clay[J]. Rock and Soil Mechanics, 2016, 37(4): 973–980.

[18] WEI Li-min, ZHANG Chao-fan, ZHAI Shun, et al. Analysis of lateral cyclic loaded pile considering weakening effect of *m* value[J]. Journal of Central South University (Science and Technology), 2018, 49(9): 2272–2279.

[19] HU An-feng, NAN Bo-wen, CHEN Yuan, et al. Modified *p-y* curves method based on degradation stiffness model of sand[J]. Journal of Shanghai Jiao Tong University, 2020, 54(12): 1316–1323.

[20] RATHOD D, MUTHUKKUMARAN K, THALLAK S G. Experimental investigation on behavior of a laterally loaded single pile located on sloping ground[J]. International Journal of Geomechanics, 2019, 19(5): 04019021.

[21] CCCC Highway consultants Co., Ltd. JTG 3363－2019

Specifications for design of foundation of highway bridges and culverts[S]. Beijing: China Communications Press, 2019.

[22] HONG Y, HE B, WANG L, et al. Cyclic lateral response and failure mechanisms of semi-rigid pile in soft clay: centrifuge tests and numerical modelling[J]. Canadian Geotechnical Journal, 2017, 54(6): 806–824.

[23] HONG Y, HE B, WANG L, et al. Cyclic lateral response and failure mechanisms of semi-rigid pile in soft clay: centrifuge tests and numerical modelling[J]. Canadian Geotechnical Journal, 2017, 54(6): 806–824.

[24] MUTHUKKUMARAN K, SUNDARAVADIVELU R, GANDHI S R. Effect of slope on *p-y* curves due to surcharge load[J]. Soils and Foundations, 2008, 48(3): 353–361.

[25] NG C W W, ZHANG L M. Three-dimensional analysis of performance of laterally loaded sleeved piles in sloping ground[J]. Journal of Geotechnical and Geoenvironmental Engineering, 2001, 127(6): 499–509.

[26] NIMITYONGSKUL N, KAWAMATA Y, RAYAMAJHI D, et al. Full-scale tests on effects of slope on lateral capacity of piles installed in cohesive soils[J]. Journal of Geotechnical and Geoenvironmental Engineering, 2018, 144(1): 04017103.